DOI: 10.1021/ma900942j

Macromolecules
ARTICLE

Array of Magnetic Nanoparticles via Particle Co-operated Self-Assembly in Block Copolymer Thin Film

Mottakin M. Abul Kashem,[†,‡] Jan Perlich,[†,‡] Alexander Diethert,[†] Weinan Wang,[†] Mine Memesa,[§] Jochen S. Gutmann,[§] Eva Majkova,[⊥] Ignác Capek,[∥] Stephan V. Roth,[‡] Winfried Petry,[†,#] and Peter Müller-Buschbaum*[,†]

[†]*Physik-Department LS E13, Technische Universität München, James-Franck-Strasse 1, Garching, Germany,* [‡]*HASYLAB at DESY, Notkestrasse 85, 22603 Hamburg, Germany,* [§]*Max Planck Institute for Polymer Research, Ackermannweg 10, 55128 Mainz, Germany,* [⊥]*Institute of Physics SAS, Dúbravská 9, SK 84511 Bratislava, Slovakia,* [∥]*Polymer Institute, SAS, Dúbravská 9, SK 84236 Bratislava, Slovakia, and* [#]*Forschungsneutronenquelle Heinz Maier-Leibnitz, Technische Universität München, Lichtenbergstrasse 1, 85747 Garching, Germany*

Received April 30, 2009; Revised Manuscript Received July 10, 2009

ABSTRACT: The influence of nanoparticles on the domain orientation in a particle co-operated self-assembly process in thin diblock copolymer films is investigated toward the preparation of ordered magnetic nanoparticle arrays. Thin films are prepared from a mixture of chemically masked iron oxide nanoparticles and a polystyrene-*block*-poly (methyl methacrylate) diblock copolymer. The resulting nanostructures are investigated with grazing incidence small-angle X-ray scattering, atomic force microscopy and scanning electron microscopy. Nanoparticles arrange themselves spontaneously inside the upright cylindrical domains due to the selective affinity to the poly (methyl methacrylate) minority phase during the microphase separation process and due to the balance of the surface free energies between the polymers and the nanoparticle coating after annealing. The incorporation of the nanoparticles inside the cylindrical domains increases the diameter of the cylindrical domains and the distance between two neighboring domains. A spatially ordered arrangement of magnetic nanoparticles is observed below a critical concentration of 0.2 vol % for the investigated molecular weight of 77 kg/mol.

1. Introduction

Block copolymers are attracting continuously strong interest in fundamental research as well as in technological applications due to the formation of mesoscopic lattice structures through microphase separation. New generation hybrid materials based on such a self-assembly process in a block copolymer are now receiving more and more attention for electronic, magnetic, optical, biological, and chemical sensor applications.[1−9] Spontaneously formed, microphase-separated, long-ranged ordered diblock copolymer nanostructures can act as the template for an ordered arrangement of inorganic nanoparticles for target applications.[10−16] The essential very first step in these approaches is the template preparation. Controlled orientation of the domains in the microphase separated block copolymer film is very important to prepare such a template. Common methods to get controlled orientation of domains in microphase separated block copolymer films are using electric fields,[1,17] solvent annealing,[18,19] chemically patterned substrate,[20,21] shear,[22] and controlled interfacial interaction.[23,24] One common technique is the removal of one block from the film followed by filling with the desired materials.[1,5,12,18,19,25] Vapor deposition of metal,[19] dip-coating from a nanoparticle dispersion,[26] and electrophoretic deposition[27] on to the porous template can produce an array of inorganic nanostructures, too.

Coupling a self-assembly processes with a spatial arrangement of nanoparticles due to preferential interaction is a promising technique to establish ordered structures of the nanoparticles and its clusters.[6,8,10,28−32] The basic idea is to tailor the surface chemistry of the nanoparticles so that they arrange themselves inside a preferential domain. In this present study, we have focused on few fundamental issues regarding such kind of particle co-operated self-assembly in a thin film of a diblock copolymer. For example, is there any limit of incorporation of nanoparticles? What happens to the size and distances of the domain structures? Is there any effect of nanoparticles on the domain orientation? We have used a model system comprising of a polystyrene-*block*-poly (methyl methacrylate) diblock copolymer and iron oxide nanoparticles coated with oleic acid and oleyl amine to produce an array of magnetic domains. The nanostructures which are present in the films due to microphase separation and spatial arrangement of nanoparticles are investigated by the real-space techniques atomic force microscopy and scanning electron microscopy and by the reciprocal-space technique grazing incidence small-angle X-ray scattering (GISAXS).

2. Experimental Section

Sample Preparation. The used polystyrene-*block*-poly (methyl methacrylate) diblock copolymer P(S-*b*-MMA) with a molecular weight of $M_w = 77$ kg/mol and a polydispersity of 1.09 (M_w/M_n) was purchased from Polymer Source Inc. (volume fraction of the PMMA block is 0.29). Iron oxide nanoparticles were synthesized by a high temperature solution-phase reaction of metal acetylacetonates ($Fe(acac)_3$) with oleic acid and oleyl amine. Details of the procedure are described elsewhere.[33] The diameter of the nanoparticles was $D_{np} = (6.4 \pm 0.6)$ nm and the average interparticle distance in a self-assembled hexagonal-closed packed array was $d_{np} = (7.7 \pm 0.6)$ nm on top of a hydrophobic silicon (100) substrate. The substrates were immersed in 19% hydrofluoric acid for 2 min at room temperature, followed by a

*Corresponding author. Telephone: +49 89 289 12451. Fax: +49 89 28912473. E-mail: muellerb@ph.tum.de.

 Published on Web 07/24/2009

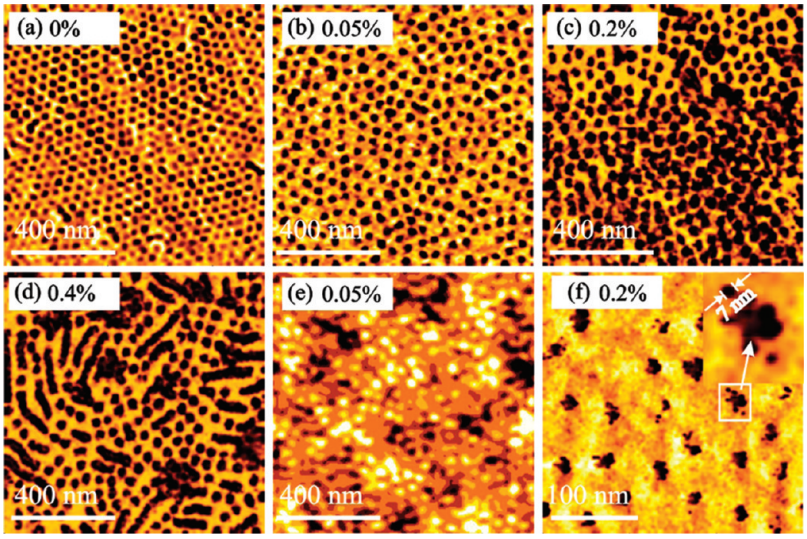

Figure 1. AFM images showing (a, b, c, d, and f) phase contrast and (e) height of the surfaces of microphase separated P(S-*b*-MMA) diblock copolymer films containing varying amount of magnetic nanoparticles on top of silicon (100). The scan area is 1 μm × 1 μm for images a−e and 0.3 μm × 0.3 μm for image f. Percentages shown in the figures correspond to the respective nanoparticle concentration in vol %. The hexagonally packed perpendicularly oriented cylindrical domains of PMMA in PS matrix are quite distinct in part a. Upon addition of small amount of nanoparticles the hexagonal packing is distorted (b and c). The height image does not show the presence of nanoparticles on top (e). Addition of more nanoparticles (d) creates clusters. Nanoparticle clusters are located inside the cylindrical domains (f). Inset of part f shows the magnified view of one cluster and single nanoparticle of ~7 nm diameter. The height scale bar range is 1.5 nm.

strong rinsing with deionized water and nitrogen gas drying. The thicknesses of all films containing varying amount (0%, 0.05%, 0.1%, 0.2%, 0.4%, and 0.8% by volume (vol) of the amount of polymer in solution) of nanoparticles were $l \sim 82$ nm. One set of samples was annealed at 165 °C in a vacuum oven (1×10^{-3} mbar) for 72 h and another identical set was investigated without annealing. During annealing upright cylindrical domains of PMMA in a PS matrix form through microphase separation.[34]

Atomic Force Microscopy (AFM). Local surface structures were investigated with an atomic force microscope (AFM) in tapping mode operating an Autoprobe CP research AFM instrument. The used gold-coated silicon cantilevers (Ultralever cantilevers) had a resonance frequency of 60 kHz, a tip with a high aspect ratio and an asymptotic conical shape. The measurements were performed at room temperature in air. Each scanned height and phase micrograph consists of 256 lines, scanned with 0.25 Hz up to 1.0 Hz. From the raw data, the background due to the scanner-tube movement was fully subtracted.

Scanning Electron Microscopy (SEM). Scanning electron microscopy (SEM) was performed on selected samples using field emission SEM (Zeiss LEO 1530 "Gemini") operated at an acceleration voltage of 1 KV to 3 KV with the lateral resolution of up to 1 nm. All images were taken with the secondary electrons detector. The samples were investigated without staining. The working distance was 1 mm.

Grazing Incidence Small-Angle X-ray Scattering (GISAXS). GISAXS measurements were carried out at the beamline BW4 of the DORIS III storage ring at HASYLAB (DESY, Hamburg, Germany). The selected wavelength was $\lambda = 0.138$ nm. The beam was focused to the size of < 60 μm × 30 μm. The sample was placed horizontally on a goniometer. A beam stop was used to block the direct beam in front of the detector. Besides, a second, rod-like moveable beam stop was sometimes also used to block the very high specular intensity on the detector. The incident angle was set to $\alpha_i = 0.31°$, which is well above the critical angles of the blocks of the polystyrene-*block*-poly (methyl methacrylate) diblock copolymer (PS 0.138° and PMMA 0.146°) and nanoparticles (0.28°). Therefore, the X-ray beam penetrates the whole film and the scattering data gives the information of the structural lengths present in the full depth of the film. The scattered intensities were recorded by a 2D detector (MARCCD; 2048 × 2048 pixel) positioned at a distance $D_{SD} = 2.095$ m behind the sample. Due to the shallow incident angle, the footprint of the X-ray beam on the sample surface was 5.5 mm long. Therefore, the statistics of the nanostructures information is increased by a factor of 1000 compared to AFM and SEM.

3. Results and Discussion

a. Local Surface Structures. Figure 1 shows the surface structures of polystyrene-*block*-poly (methyl methacrylate) diblock copolymer films containing different volume fractions of nanoparticles investigated with tapping mode AFM. Figure 1a shows microphase separated cylindrical domains (dark phase) of PMMA arranged in a PS matrix. Only honeycomb-like structures are visible because the cylinders are oriented perpendicular to the substrate and AFM shows the top view. These cylindrical domains have an average diameter of 30 ± 2 nm. The upright cylindrical PMMA domains in the PS matrix are produced by decreasing the surface energy of the substrate by the HF acid treatment. This treatment makes the substrate hydrogen passivated and ultrahydrophobic, which results in a similar affinity to both blocks in the investigated block copolymer.[34] As a result, during spin coating, the upright cylindrical domains are formed and long-ranged order is established by a subsequent annealing at above the glass transition temperature (T_g) of both blocks (T_g of PS is 100 °C and T_g of PMMA is 105 °C). This long-range ordered structure is perturbed when a small amount of nanoparticles is added.

There is no more hexagonal packing present in that sample, shown in Figure 1b. An increase in diameter of the cylinders from 30 ± 2 to 37 ± 2 nm is also observed. This increase is because of selective incorporation of the nanoparticles in the PMMA phase and the space required by the oleic acid ligands attached to the metal oxide nanoparticles. The nanoparticles were stabilized against agglomeration in toluene by grafting oleyl amine and oleic acid. The surface tension of both domains at the substrate- and air-interface should be the same in order to form upright cylinders. For that reason, the coating of the nanoparticles also prefers the PMMA phase to have a balanced interfacial tension since the surface tension of PS, PMMA and hydrocarbons are

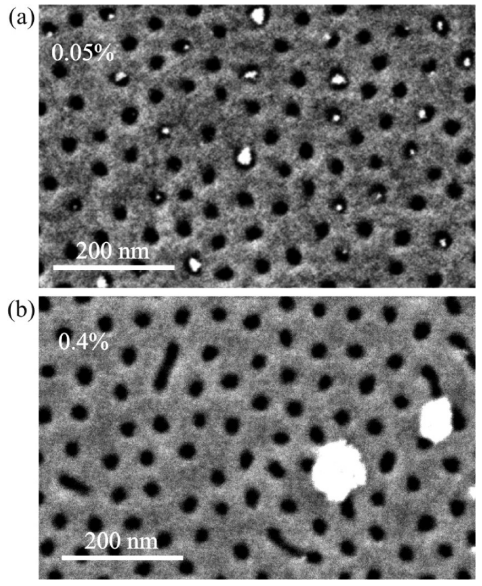

Figure 2. SEM micrographs of P(S-*b*-MMA) diblock copolymer thin films containing (a) 0.05 and (b) 0.4 vol % nanoparticles. At a low concentration of nanoparticles the clusters (bright objects) are located in the cylindrical PMMA (dark phase) domains (a). At higher concentration (b), big clusters are not selectively present in PMMA domains anymore.

$\sim$ 39, $\sim$ 41, and 29 mN m^{-1}, respectively.[35,36] Besides, the iron oxide binds to PMMA via carboxylate anion and hydrogen bonding, which was reported before.[37] As a result, during the self-assembly process the nanoparticles arrange themselves inside the PMMA domains resulting in an increased domain size. However, it is not clear from Figure 1b whether the particles are located inside the polymer film or on top of the surface. The height image of the same sample surface shown in Figure 1e exhibits no significant height changes due to the presence of nanoparticles (the color scale bar has the range of 1.5 nm). With a reduced scan size, the presence of nanoparticles is easily observed and the size of the nanoparticles can be extracted to be 7 nm (see Figure 1f). Moreover, the particles form clusters inside the PMMA domains. With increasing nanoparticle concentration, the cluster size increases and the long-range ordered upright cylinders loose their ordered arrangement. Above the critical volume fraction (0.2%, see Figure 1c) big clusters of nanoparticles are observed. The presence of these clusters causes a mixed orientation of the PMMA domains in the PS matrix, which is visible in Figure 1d.

For imaging the spatial arrangement of the nanoparticles in the thin film selected samples were investigated with scanning electron microscopy (SEM). Figure 2 presents SEM images of two different films with a low (0.05 vol %) and a high (0.4 vol %) amount of nanoparticles. The dark circular phases are the cylindrical domains of PMMA, the bright objects inside the PMMA cylinders are the nanoparticle clusters of different size, and the third gray matrix is the PS. It is clear from Figure 2a that nanoparticle clusters having a size smaller than the diameter of the cylinders distribute themselves in the cylinders at very low concentration by a particle co-operated self-assembly process.[10] When the concentration of the nanoparticles is high enough to form clusters bigger than the diameter of the cylinders, these clusters cannot be accommodated in the cylinders. In such a case, the underlying self-assembled diblock copolymer structure is no longer correlated with the nanoparticle assembly (see Figure 2b).

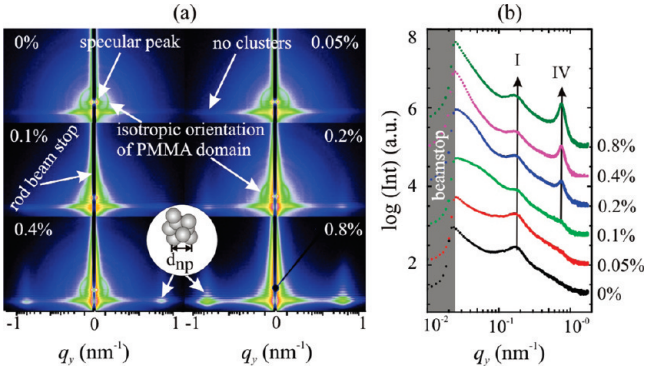

Figure 3. (a) 2D GISAXS patterns and (b) out-of-plane cuts of as-prepared films containing different volume concentrations of nanoparticles. The intensity scale is chosen logarithmic. The percent numbers given correspond to the nanoparticle concentration in the respective patterns (a) and cuts (b). The cuts are shifted along the *y*-direction for a better comparison with others. The structure factor peak denoted with **I** arise from the cylinder-to-cylinder distance $d_{cyl} = (37 \pm 7$ nm and the one denoted with **IV** from the interparticle distance, $d_{np} = 8 \pm 1$ nm.

Because the penetration depth of the electrons in SEM is approximately 10 nm the images show not only the surface features but also the volume within this 10 nm depth. This means the visualized nanoparticles have to be located within a distance of 10 nm to the surface. However, a more precise determination of the nanoparticles position along the surface normal is not possible with SEM.

b. Nanostructures Inside the Film. To get more details of the lateral structures present inside the films, the as-prepared and the annealed films are investigated with GISAXS. Details of the GISAXS technique are described elsewhere.[38] The used incident angle ($\alpha_i = 0.31°$) of the X-ray beam was chosen well above the critical angle of both blocks of the diblock polymer, PS (0.138°) and PMMA (0.146°), and of the nanoparticles ($\alpha_c < 0.28°$) for the wavelength used ($\lambda =$ 0.138 nm). Therefore, the beam penetrates the full depth of the film and the 2D scattering patterns give an average of the structural information present on the surface and inside the film. This structural information contains both, the in-plane and out-of-plane direction.

As-Prepared Films. Figure 3 shows GISAXS patterns recorded on a 2D detector and the out-of-plane cuts containing the important lateral length information for different amounts of nanoparticles in the as-prepared films. All scattering patterns are quite similar and have a ring of intensity with the specular peak at their center except the one with 0.8 vol % nanoparticles. Such a ring of intensity in a GISAXS pattern represents the isotropic orientation of the domains in the film.[39] Therefore it is a clear indication of the presence of randomly oriented domains of PMMA in the PS matrix. Along with the ring of intensity, the films have also intensity side maxima at almost similar values of q_y. Only films having a nanoparticle volume fraction of more than 0.1% exhibit intensity side maxima at other positions of q_y. The vertical modulation present in these side maxima is due to the interface correlation.[40−42] The positions of the side maxima are obtained by making out-of-plane cuts at q_z values equivalent to the critical angle of PS. All the cuts are plotted in Figure 3b. One type of intensity side maxima, denoted with **I,** appears at a position of $q_y = 0.168$ nm^{-1}. The position of this peak is constant in all films, which is indicated by a black arrow. The corresponding real-space length is 37 ± 7 nm, which is the distance between neighboring cylinders, d_{cyl}. This peak appears due to the presence of upright cylindrical domains in the film. The second peak,

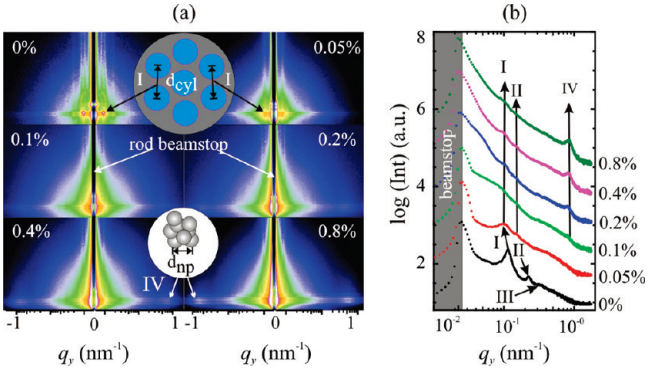

Figure 4. (a) 2D GISAXS patterns and (b) out-of-plane cuts of annealed films containing varying volume concentrations of nanoparticles. The intensity scale is chosen logarithmic. The percent numbers given correspond to the nanoparticle concentration in the respective patterns (a) and cuts (b). The cuts are shifted along the *y*-direction for a better comparison with others. The structure factor peaks denoted with **I**, **II**, and **III** arise from the cylinder-to-cylinder distance d_{cyl} and the one denoted with **IV** from the interparticle distance, d_{np}.

denoted with **IV,** appears at higher values of $q_y = 0.584$ nm^{-1} only in the films with a nanoparticle volume fraction of more than 0.1%. The lateral distance corresponding to this peak position is 8 ± 1 nm, which is the distance between two neighboring nanoparticles in clusters i.e. d_{np}. Because all films show equal lateral structural lengths, it is clear from the GISAXS data that the nanoparticles do not arrange spatially inside the PMMA domain in as-prepared films before annealing. If the nanoparticles would arrange inside the PMMA domain, the size of the domains would increase and the lateral distances among domains would increase, as a consequence. The distance between two adjacent spherical nanoparticles in a cluster is given by the diameter of a single nanoparticle. Therefore, the structure factor in the scattering pattern of the cluster of nanoparticles gives directly the diameter of the nanoparticles.

Annealed Films. After annealing, the film morphology changes as revealed by GISAXS and AFM. The 2D GISAXS scattering pattern of the sample without nanoparticles (see Figure 4a, top left) shows three side maxima (denoted with I, II, and III) which are oriented in parallel to the scattering plane (see Figure 4b). The highly ordered array of cylindrical PMMA domains, shown in Figure 1a, causes these side maxima, which are maxima of the structure factor. The electron density contrast between the two phase-separated domains (PMMA and PS) causes the visibility of the structure factor maxima. Due to the high degree of order of the array the first, second and third order Bragg peaks are visible. The in-plane lengths corresponding to theses side maxima are **I** = 55 nm, **II** = 30 nm, and **III** = 19 nm. The ratio of these values is **I**:**II**:**III** = 1:1/$\sqrt{3}$:1/$\sqrt{7}$, which indicates a hexagonal order of the polymer. Thus the diblock copolymer film without nanoparticles consists of highly ordered, hexagonally packed, upright cylindrical domains of PMMA in the PS matrix. The addition of a tiny amount of nanoparticles (0.05 vol %) did not destroy the orientation of the PMMA cylinders. Still two side maxima are clearly visible in the GISAXS pattern of the corresponding sample. Thus from the structure factor of the cylinder array two Bragg peaks are observed. As observed with AFM, the distances among the cylinders are not as regular as in the sample without nanoparticles (compare parts a and b of Figure 1), which produces a broadly distributed peak of second order and results in the absence of the third order peak. The very interesting and most important fact is the change of the position of the peaks **I** and **II**. As shown in Figure 4 both peaks shift toward smaller q_y values caused by an increase of lateral distances among the cylindrical domains of PMMA. Thus, the incorporation of only 0.05 vol % nanoparticles inside the cylinders causes a lateral swelling of the domains of PMMA already. As a result, the corresponding structure factor, arising from the cylinder-to-cylinder distance d_{cyl}, shifts toward lower value in reciprocal space as the distance d_{cyl} increases. The presence of nanoparticles only inside the PMMA domains is shown in Figure 1f and 2a for the surface as well. Therefore, at a value of 0.05 vol % nanoparticle concentration the nanoparticles are located purely inside the PMMA phase in the entire film and at the film surface, which consists of upright cylindrical domains.

With increasing the volume fraction of nanoparticles (0.1−0.8 vol %) the positions of the peaks **I** and **II** remain constant in the GISAXS data (indicated in Figure 4b with two black arrows). Correspondingly, no further swelling of the PMMA domains due to the increased addition of nanoparticles occurs. Moreover, with an increasing amount of added nanoparticles an additional side maximum appears (see Figure 4). The related structure factor peak, denoted with **IV,** arises from the distances between two neighboring nanoparticles. At a low volume fraction of nanoparticles (0.05 and 0.1 vol %) only a shoulder-like feature in the horizontal cut of the GISAXS intensity is observed instead of this pronounced peak. At 0.2 vol % of nanoparticles, a weak peak becomes visible, which increases its intensity with increasing nanoparticle concentration. However, the q_y-position of the peak remains constant. The corresponding real space lateral length is (8 ± 1) nm, which is almost equal to the interparticle distance i.e., the center-to-center distance of nanoparticles in a hexagonal closed packed monolayer.[33] As a consequence, the occurrence of the structure factor peak **IV** is related with the presence of densely packed nanoparticles. Obviously, at 0.05 and 0.1 vol % mostly isolated nanoparticles occur. At a critical concentration of 0.2 vol % the nanoparticles start forming clusters. These clusters are bigger than the size of the diameter of the PMMA cylinders and therefore, distribute randomly in the whole film, which gives rise to the scattering intensity at the peak position **IV**. Such behavior is in good agreement with the morphologies seen in the SEM images (e.g., of the sample containing 0.4 vol % nanoparticles shown in Figure 2b).

To confirm additionally the in-plane and out-of plane spatial distribution of the nanoparticles, detector cuts[38] have been made from the 2D GISAXS patterns of the annealed films which were measured using a GISAXS setup with a point-shaped beamstop instead of the rod-shaped beamstop. Thus only the specular peak is blocked and the intensity at $q_y = 0$ is accessible. These detector cuts are presented in Figure 5 as a function of the volume fraction of the iron oxide nanoparticles. The positions of the specular peaks (marked by thick black solid line in Figure 5) and the Yoneda peaks[43] arisen from the PS matrix of the copolymer films remain constant with increasing amount of nanoparticles. The first Yoneda peak appears at an in-plane scattering angle $\phi = 0.448°$ ($\alpha_i + 0.138°$), which is exactly at the critical angle of PS ($\alpha_c = 0.138°$) for the used X-ray wavelength. This means the density of the matrix phase, which is PS, remains constant with the addition of iron oxide nanoparticles having an approximately five times higher density. An opposite scenario is observed with the second Yoneda peak at $\phi = 0.458°$ ($\alpha_i + 0.146°$), which corresponds to the critical angle of the PMMA domains. The position of this Yoneda peak shifts toward higher angles as the volume fraction of the nanoparticles increases. This increase in critical angle corresponds to the increase of the

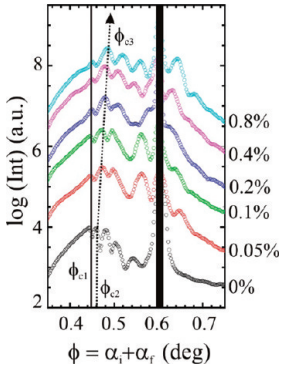

Figure 5. Detector cuts of the annealed films of different volume concentration of nanoparticles are extracted from 2D GISAXS patterns measured with a point-shaped instead of the rod-shaped beamstop. The specular peak is blocked (shown by the thick solid black line). The percent numbers given correspond to the volume fractions of the nanoparticles in the respective cuts. The cuts are shifted along the *y*-direction for a better comparison with others. ϕ, α_i, and α_f are the in-plane scattering angle, the incident angle and the exit angle, respectively. ϕ_{c1}, ϕ_{c2}, and ϕ_{c3} are the in-plane scattering angles (Yoneda peak positions) at the exit angles $\alpha_f = \alpha_c$(PS), $\alpha_f = \alpha_c$(PMMA) and $\alpha_f = \alpha_c$(PMMA + np), respectively with α_c is the critical angle. The thin solid line shows the constant position of the Yoneda peak at $\alpha_f = \alpha_c$(PS). The dotted lines show the increase of the critical angle of the PMMA with the increasing volume fractions of iron oxide nanoparticles.

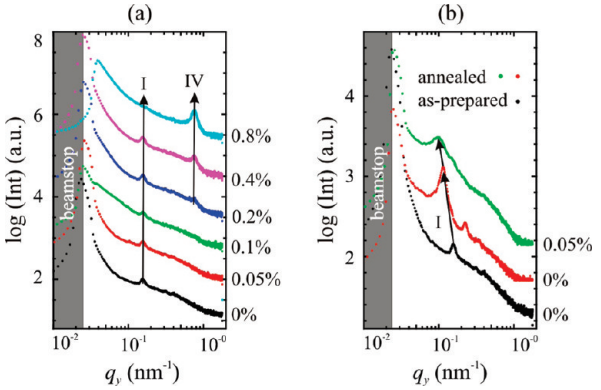

Figure 6. (a) Out-of-plane cuts at the position of specular peaks of GISAXS patterns of as-prepared films with varying amount of nanoparticles. Peak **I** arises from the structure factor representing the cylinder-to-cylinder distance $d_{cyl} = 40 \pm 3$ nm and peak **IV** represents the interparticle distance $d_{np} = 8 \pm 1$ nm. The percent numbers next to the cuts are the nanoparticle concentrations. (b) A comparison of out-of-plane cuts of the as-prepared and the annealed films containing 0% nanoparticles and the annealed film with 0.05 vol % nanoparticles. The increase of the distance d_{cyl} due to annealing and incorporation of nanoparticles is revealed as the shift of the position of the peak **I** to the lower value of q_y.

average electron density of the PMMA domains. Since this increase in the critical angle happened only for the PMMA domains, it is certain that the iron oxide nanoparticles are allocated inside the PMMA domains only. Thus, these detector cuts are in good agreement with the structure deduced from AFM, SEM, and the GISAXS out-of-plane cuts.

c. Effect of Annealing on the Spatial Arrangement of the Nanoparticles. One fundamental issue is to know when the spatial arrangement of the nanoparticles inside the PMMA domains occurs. Comparing the GISAXS data of the as-prepared and annealed films, it is observed that the spatial arrangement of the nanoparticles inside the domains occurs during annealing. To make it more clear the out-of-plane cuts from the GISAXS patterns of the as-prepared and the annealed films without nanoparticles are compared with that of the film containing 0.05 vol % nanoparticles in Figure 6b. The position of peak **I** shifts to a lower value of q_y upon annealing the film without nanoparticles, which is because of the increase of the distance between two neighboring cylinders d_{cyl} from 40 to 55 nm. The addition of 0.05 vol % nanoparticles increases again this distance d_{cyl} to 65 nm. However, the as-prepared film with the same nanoparticle concentration exhibits a distance of $d_{cyl} = 40$ nm.

For a better comparison, the out-of-plane cuts at the specular peak position of all as-prepared samples are shown in Figure 6a as well. The position of peak **I** does not change with increasing nanoparticle concentration at all. The corresponding real-space length is 40 ± 3 nm. If the nanoparticles would have been allocated inside the PMMA domains before annealing, the distance d_{cyl} would have changed because more nanoparticles require more space in the cylinder domain and the structure has to swell to accommodate nanoparticles. Therefore, it is quite certain that the nanoparticles arrange themselves spatially in the PMMA domains only during the annealing process. The nanoparticles balance the interfacial energy difference between PS and PMMA[10] although the interfacial energy difference between PS and PMMA is very low. Besides, the interaction between the iron oxide core of the nanoparticles and PMMA via carboxylate and hydrogen bonds is well-known.[36]

These interactions drive the nanoparticles to locate inside the PMMA domain. As a result of these physical and chemical driving forces, the spatial arrangement of iron oxide nanoparticles inside the PMMA domain is achieved. The migration of the nanoparticles can only occur when the film is not glassy and the chains are mobile. During thermal annealing, the polymer chains get sufficient thermal energy to be mobile, which allows the nanoparticles to migrate to the PMMA domain. Before annealing the structures present in the film are frozen and so no migration is possible.

d. Effect of Annealing and Nanoparticles on Domain Orientation. To understand the process of the spatial arrangement of the nanoparticles inside the domains, it is necessary to observe the change of the domain orientation due to the annealing and addition of nanoparticles. The 2D GISAXS patterns of the samples with and without nanoparticles are compared in Figure 7. Before annealing, the samples do not have a perpendicular orientation of the PMMA domains although they were spin coated on top of the hydrogen passivated silicon surface. The interfacial energy between the polymer and the substrate was not sufficient to orient the PMMA domains in the whole film. Randomly oriented PMMA domains are frozen by the evaporation of the solvent during spin coating. The ring of the intensity around the specular peak in the 2D GISAXS patterns represents this isotropic orientation of the domains.[39] Thus, the nanoparticles do not arrange spatially at this stage of preparation. All the isotropic structures with and without nanoparticles are similar before annealing. There is no change in average domain spacing due to addition of nanoparticles. As explained above, this is a clear indication of the random arrangement of the domains and the particles.

The situation changes dramatically after annealing. The film without nanoparticles shows a hexagonally packed, perpendicular orientation on the surface of the film (shown in Figure 1a). Nevertheless, the internal orientation, which cannot be resolved with AFM, is not the same all through the entire film. There are few grains of different orientation present inside the film. This produces a ring of weak intensity in the 2D GISAXS data of the sample without nanoparticles after annealing shown in Figure 7c. However, the presence of higher order Bragg peaks (rods), representing

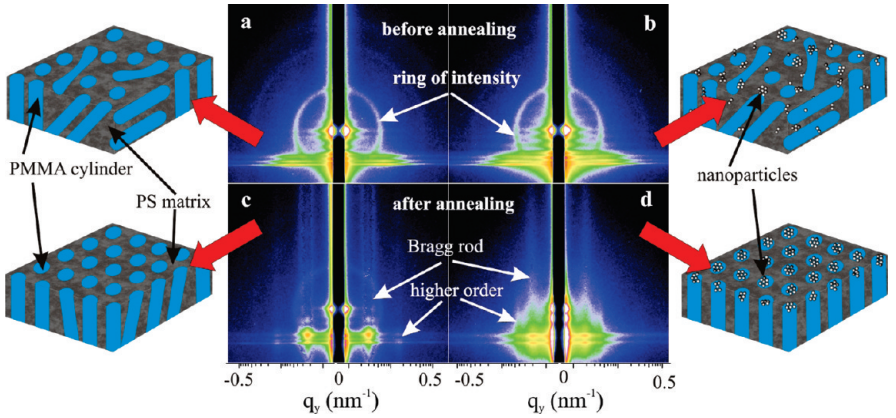

Figure 7. 2D GISAXS patterns of P(S-*b*-PMMA) thin films without nanoparticles (a, c) and with nanoparticles (b, d), are before annealing (a, b) and are after annealing (c, d): The intensity is shown in logarithmic scale. The schematic diagrams indicate the corresponding domain orientations and nanoparticles arrangement in real space. The strong ring of intensity around the specular peak in unannealed films presents an isotropic orientation of PMMA domains in PS matrix. The appearance of Bragg rods with higher order in annealed films indicates the perpendicular orientation of PMMA domains.

the cylinder-to-cylinder distance, indicates that most of the film has a perpendicular orientation of hexagonally packed PMMA cylinders in PS. The interdomain spacing increases from 40 to 55 nm due to the ordered packing. A fully perpendicular orientation is achieved for the sample with 0.05 vol % nanoparticles after annealing. As outlined above, physical and chemical driving forces cause the nanoparticles to locate inside the PMMA domains. As a result, the perpendicular orientation of the PMMA cylinders throughout the whole film is achieved (disregarding small defects). The presence of nanoparticles inside the PMMA domains increases the domain size and the cylinder-to-cylinder distance. The strong increase at low nanoparticle concentrations can result from the surface coating of the nanoparticles with oleyl acid ligands and the space requirement of the ligands. Because the mobility of the PMMA chains is restricted by the interaction with the iron oxide nanoparticles, only a short-range ordered hexagonal array is observed. The nanoparticle clusters form in samples with a higher amount of nanoparticles (0.2 vol % and above) during spin coating because they are observed in annealed and in as-prepared samples. This cluster formation process is described in our earlier work.[6,40] During annealing, the clusters, which are larger than the diameter of a cylinder, can not accommodate in the PMMA domain because of the lack of enthalpy. Below the critical concentration, 0.2 vol %, the cluster sizes are small enough for a spatial arrangement inside the PMMA domains.

Therefore, in order to have a controlled lateral arrangement of the nanoparticles inside the microphase separated block copolymer domain, the amount of nanoparticles inside the polymer film should not exceed the critical concentration limit of 0.2 vol %. Below this critical concentration, the domains of PMMA can selectively accommodate the iron oxide nanoparticles for the chosen molecular weight of the diblock copolymer and thus, a regular array of magnetic nanoparticles can be obtained (schematic view in Figure 7d).

4. Conclusion

We have investigated the influence of iron oxide nanoparticles and annealing on the PMMA domain orientation in P(S-*b*-MMA) diblcok copolymer films resulting in an ordered arrangement of nanoparticles through a particle co-operated self-assembly process. This systematic investigation of the nanostructures in the whole film at different nanoparticle concentrations before and after annealing by real-space and reciprocal-space analysis techniques proved the possibility to produce an ordered arrangement of nanoparticles below a critical concentration limit of 0.2 vol % for the investigated molecular weight of 77 kg/mol. Below this volume fraction, the surface free energies of the particles, the particle coating and the matrix polymers and the ionic interaction and the hydrogen bonding between the particles and the carboxylic group in PMMA play important roles for the selective positioning of the nanoparticles. Before annealing, the nanoparticles do not arrange inside the PMMA domains. During the annealing, nanoparticles arrange themselves spatially inside the PMMA domains. The incorporation of nanoparticles inside the PMMA domains increases the domain size and the lateral spacing by a swelling process at very low volume concentrations. This increase can result from the surface coating of the nanoparticles with oleyl acid ligands. A magnetic interaction is unlikely at the very low concentrations to contribute to the domain swelling. Besides, the presence of nanoparticles inside the PMMA domains also leads to a perpendicular orientation through balancing the interfacial energies between the polymer blocks at the substrate interface. Thus, this detailed investigation points out the strengths and limitations of the particle co-operated self-assembly process in thin diblock copolymer films. With a proper selection of the block copolymers and nanoparticles one can fabricate nanostructured materials for potential applications in chemical sensors, biosensors, catalysts, chemical separation, photonic materials, and high-density data storage devices.

Acknowledgment. We thank HASYLAB, DESY, Hamburg, Germany for providing the facilities to use synchrotron radiation source for GISAXS experiment. This work was financially supported by Deutsche Forschungsgemeinschaft (DFG) in the priority program SPP1181 "NanoMat" (MU 1487/5 and GU 771/2) and by the Bavarian State Ministry of Sciences, Research and the Arts through the international doctorate school ComplInt.

References and Notes

(1) Thurn-Albrecht, T.; Schotter, J.; Kastle, C. A.; Emley, N.; Shibauchi, T.; Krusin-Elbaum, L.; Guarini, K.; Black, C. T.; Tuominen, M. T.; Russell, T. P. *Science* **2000**, *290*, 2126.
(2) Shenton, W.; Pum, D.; Sleytr, U. B.; Mann, S. *Nature* **1997**, *389*, 585.
(3) Bockstaller, M.; Kolb, R.; Thomas, E. L. *Adv. Mater.* **2001**, *13*, 1783.
(4) Mann, S.; Ozin, G. A. *Nature* **1996**, *382*, 313.

(5) Darling, S. B.; Yufa, N. A.; Cisse, A. L.; Bader, S. D.; Sibener, S. J. *Adv. Mater.* **2005**, *17*, 2446.
(6) Abul Kashem, M. M.; Perlich, J.; Schulz, L.; Roth, S. V.; Petry, W.; Müller-Buschbaum, P. *Macromolecules* **2007**, *40*, 5075.
(7) Alexandre, M.; Dubois, P. *Mater. Sci. Eng. Rev.* **2000**, *28*, 1–63.
(8) Lauter-Pasyuk, V.; Lauter, H. J.; Gordeev, G. P.; Müller-Buschbaum, P.; Toperverg, B. P.; Petry, W.; Jernenkov, M.; Petrenko, A.; Aksenov, V. *Physica B* **2004**, *350*, e939.
(9) Roth, S. V.; Walter, H.; Burghammer, M.; Riekel, C.; Lengeler, B.; Schroer, C.; Kuhlmann, M.; Walther, T.; Sehrbrock, A.; Domnick, R.; Müller-Buschbaum, P. *Appl. Phys. Lett.* **2006**, *88*, 021910.
(10) Lin, Y.; Böker, A.; He, J.; Sill, K.; Xiang, H.; Abetz, C.; Li, X.; Wang, J.; Emrick, T.; Lung, S.; Wang, Q.; Balazs, A.; Russell, T. P. *Nature* **2005**, *434*, 55.
(11) Minelli, C.; Geissbuehler, I.; Eckert, R.; Vogel, H.; Heinzelmann, H.; Liley, M. *Colloid Polym. Sci.* **2004**, *282*, 1274.
(12) Kim, H.-C.; Jia, X.; Stafford, C. M.; Kim, D. H.; McCarthy, T. J.; Tuominen, M.; Hawker, C. J.; Russell, T. P. *Adv. Mater.* **2001**, *13*, 795.
(13) Chiu, J. J.; Kim, B. J.; Kramer, E. J.; Pine, D. J. *J. Am. Chem. Soc.* **2005**, *127*, 5036.
(14) Aleksandrovic, V.; Greshnykh, D.; Randjelovic, I.; Frömsdorf, A.; Kornowski, A.; Roth, S. V.; Klinke, C.; Weller, H. *ACS Nano* **2008**, *2*, 1123.
(15) Chai, J.; Buriak, J. M. *ACS Nano* **2008**, *2*, 489.
(16) Rider, D. A.; Liu, K.; Eloi, J.; Vanderark, L.; Yang, L.; Wang, J.; Grozea, D.; Lu, Z.; Russell, T. P.; Manners, I. *ACS Nano* **2008**, *2*, 263.
(17) Thurn-Albrecht, T.; DeRouchey, J.; Russell, T. P. *Macromolecules* **2000**, *33*, 3250.
(18) Kim, S. H.; Misner, M. J.; Xu, T.; Kimura, M.; Russell, T. P. *Adv. Mater.* **2004**, *16*, 226.
(19) Park, S.; Wang, J.-Y.; Kim, B.; Xu, J.; Russell, T. P. *ACS Nano* **2008**, *2*, 766.
(20) Stoykovich, M. P.; Müller, M.; Kim, S. O.; Solak, H. H.; Edwards, E. W.; de Pablo, J. J.; Nealey, P. F. *Science* **2005**, *308*, 1442.
(21) Kim, S. O.; Solak, H. H.; Stoykovich, M. P.; Ferrier, N. J.; de Pablo, J. J.; Nealey, P. F. *Nature* **2003**, *424*, 411.
(22) Villar, M. A.; Rueda, D. R.; Ania, F.; Thomas, E. L. *Polymer* **2002**, *43*, 5139.
(23) Mansky, P.; Liu, Y.; Huang, E.; Russell, T. P.; Hawker, C. J. *Science* **1997**, *275*, 1458.
(24) Drockenmuller, E.; Li, L. Y. T.; Ryu, D. Y.; Harth, E.; Russell, T. P.; Kim, H. C.; Hawker, C. J. *J. Polym. Sci., Part A: Polym. Chem.* **2005**, *43*, 1028.
(25) Darling, S. B. *Surf. Sci.* **2007**, *601*, 2555.
(26) Misner, M. J.; Skaff, H.; Emrick, T.; Russell, T. P. *Adv. Mater.* **2003**, *15*, 221.
(27) Zhang, Q.; Xu, T.; Butterfield, D.; Misner, M. J.; Ryu, D. Y.; Emrick, T.; Russell, T. P. *Nano Lett.* **2005**, *5*, 357.
(28) Lopes, W. A.; Jaeger, H. M. *Nature* **2001**, *414*, 735.
(29) Lauter-Pasyuk, V.; Lauter, H. J.; Gordeev, G. P.; Müller-Buschbaum, P.; Toperverg, B. P.; Jernenkov, M.; Petry, W. *Langmuir* **2003**, *19*, 7783.
(30) Huh, J.; Ginzburg, V. V.; Balazs, A. C. *Macromolecules* **2000**, *33*, 8085.
(31) Thompson, R. B.; Ginzburg, V. V.; Matson, M. W.; Balazs, A. C. *Macromolecules* **2000**, *35*, 1060.
(32) Thompson, R. B.; Ginzburg, V. V.; Matson, M. W.; Balazs, A. C. *Science* **2001**, *292*, 2469.
(33) Siffalovic, P.; Majkova, E.; Chitu, L.; Jergel, M.; Luby, S.; Satka, A.; Roth, S. V. *Phys. Rev. B* **2007**, *76*, 195432.
(34) Xu, T.; Kim, H.-C.; DeRouchey, J.; Seney, C.; Levesque, C.; Martin, P.; Stafford, C. M.; Russell, T. P. *Polymer* **2001**, *42*, 9091.
(35) Brandrup, J.; Immergut, E. H. *Polymer Handbook*, 3rd ed; John Wiley & Sons: New York, 1998; VI/411−VI/434.
(36) Chumpitaz, L. D. A; Coutinho, L. F.; Meirelles, A. J. A. *J. Am. Oil Chem. Soc.* **1999**, *76*, 379.
(37) Leadley, S. R.; Watts, J. F. *J. Adhes.* **1997**, *60*, 175.
(38) Müller-Buschbaum, P. *Anal. Bioanal. Chem.* **2003**, *376*, 3.
(39) Busch, P.; Posselt, D.; Smilgies, D.-M; Rauscher, M; Papadakis, C. M. *Macromolecules* **2007**, *40*, 630.
(40) Abul Kashem, M. M.; Perlich, J.; Schulz, L.; Roth, S. V.; Müller-Buschbaum, P. *Macromolecules* **2008**, *41*, 2186.
(41) Müller-Buschbaum, P.; Stamm, M. *Macromolecules* **1998**, *31*, 3686.
(42) Müller-Buschbaum, P.; Gutmann, J. S.; Lorenz, C.; Schmitt, T.; Stamm, M. *Macromolecules* **1998**, *31*, 9265.
(43) Yoneda, Y. *Phys. Rev.* **1963**, *131*, 2010.